

**RESEARCH**

# One-step Redox-induced Confined Pt Nanoparticles for Reduction of Nitroaromatics

Pan Zhang | Wanchun Guo\*

Hebei Key Laboratory of Heavy Metal Deep-Remediation in Water and Resource Reuse, School of Environmental and Chemical Engineering, No. 438 West Hebei Avenue, Yanshan University, Qinhuangdao, 066004, China.

\*Corresponding author:  
Wanchun Guo  
E-mail: wc-g@ysu.edu.cn  
Tel.: +86-0335-8387743

**ABSTRACT**

The noble metal nanoparticles sandwiched between the stable inorganic core and the thin polymer shell could not only enhance their stability, but also cut short the diffusion route of the outside reactants through polymer shell toward encapsulated noble metal nanoparticles, which has drawn great attention. However, weak compatibility among inorganic core, polymer shell, and noble metal nanoparticles makes the preparation of noble metal-confined hybrid catalysts complicated, which limits the popular application of these noble metal-based catalysts. A facile method has developed to fabricate core-shell  $\text{Fe}_2\text{O}_3$ @PEDOT/Pt nanocatalyst with tiny Pt nanoparticles highly dispersed in the polymer shell by one-step simultaneous redox deposition strategy. The confinement effect and strong coordination ability of the thin sulfur-enriched polymer shell prevents the migration and agglomeration of Pt nanoparticles during the catalytic process and improves the stability of the catalyst. The catalyst shows outstanding catalytic activity and relatively good stability towards the reduction of nitroaromatic compounds. The simple method solves the problem of poor compatibility between the inorganic core, the polymer shell, and the noble metal nanoparticles confined in the shell material to some extent. Furthermore, our strategy could be extended to one-step preparation of  $\text{Fe}_2\text{O}_3$ @Polymer@Pt hybrid materials with core-shell structure.

**KEYWORDS**

Pt nanoparticles, supported catalysts, confinement, simultaneous redox reaction, core shell structure.

**INTRODUCTION**

Supported noble metal nanocatalysts have become one of the most important liquid-phase catalysts in hydrogenation, oxidation, and coupling reactions [1-5], and so on, owing to their high activity and good recyclability. However, their high surface energy and continuous collisions with the substrate during the catalytic reactions makes noble metal nanoparticles stabilized on the support surface tend to agglomerate or detach from the supports, which reduces their catalytic activity [6-8].

In order to handle the obstacle, one of the most efficient approaches adopted is to encapsulate noble metal nanoparticles into appropriate supports to prepare confined noble metal nanocatalysts. Generally, the confined structures include yolk-shell structure [9], mesoporous structure [10-11], core-shell structure [12-13], etc. In particular, core-shell nanocatalysts with spatially confined

noble metal nanoparticles, which can make full use of core-shell synergistic effect, have attracted extensive research interest. Core-shell nanocatalysts with spatially confined noble metal nanoparticles can be divided into the following two categories: (1) noble metal@support [14] and (2) support@noble metal@support [15]. The first type of core-shell structure, in which noble metal nanoparticles are typically deeply buried, reducing the collision probability between substitute molecules and active surficial metal sites and thus leading low catalytic activity. In the second one, the noble metal nanoparticles are sandwiched between the core and the thin shell, which can solve the problem of long substrate diffusion distance to improve catalytic activity. For example, Guo et al. [16] and Zhao *et al.* [17] synthesized  $\text{Fe}_3\text{O}_4$ /PANI/Au/m-SiO<sub>2</sub> and MIL-101(Fe)@Pt@MIL-101(Fe) nanocomposites, respectively.

For the core-shell nanocatalysts with spatially confined noble metal nanoparticles, the choice of support material is

This is an open access article licensed under the Creative Commons Attribution 4.0 International License, which allows for use, distribution, and reproduction in any medium as long as the original work is properly cited. © 2023 The Authors. The International Association of Advanced Materials, Sweden, publishes Advanced Materials Letters.

also significant. The supports usually include metal oxides [18-19], SiO<sub>2</sub> [20-21], carbon materials [22], polymers [23], etc. Because of its good thermal stability, simple preparation methods, and low prices, metal oxides have become excellent candidate that serves as core. With respect to shell materials, compared with inorganic materials, organic materials have many types and abundant functional groups. Among them, conductive polymers, which possess the advantages of facile synthesis and excellent doping/dedoping property [24], are considered as suitable polymer supports for the immobilization of noble metal nanoparticles. In addition, their conductive properties are expected to realize the synergistic catalysis of noble metal nanoparticles [25-26]. However, as for core-shell nanocatalysts with spatially confined noble metal nanoparticles mentioned above, the inorganic core, the noble metal nanoparticles, and the polymer shell materials exhibit poor compatibility due to their different surface properties. Moreover, it is worth mentioning that the multistep synthesis of supports and loading procedures of noble metal nanoparticles make the whole process lengthy and complicated, and the size of noble metal nanoparticles is large which lower the activity of the catalysts. Therefore, it is still a challenge to develop small size, high activity core-shell catalysts with spatially confined noble metal nanoparticles by a simple method.

Herein, we propose a facile one-step simultaneous redox deposition strategy to fabricate Fe<sub>2</sub>O<sub>3</sub>@poly(3,4-ethylenedioxythiophene)/Pt (Fe<sub>2</sub>O<sub>3</sub>@PEDOT/Pt) core-shell nanocatalysts with spatially confined Pt nanoparticles. Firstly, there is a  $\pi$ - $\pi$  interaction between the polyvinylpyrrolidone (PVP) modified on the surface of Fe<sub>2</sub>O<sub>3</sub> and 3,4-ethylenedioxythiophene, which induces the 3,4-ethylenedioxythiophene monomers to adsorb on the surface of Fe<sub>2</sub>O<sub>3</sub>, the redox reaction between K<sub>2</sub>PtCl<sub>4</sub> and 3,4-ethylenedioxythiophene monomers makes PEDOT and Pt nanoparticles simultaneously deposited on the Fe<sub>2</sub>O<sub>3</sub> core, and at the same time a small amount of protons is generated, which makes the Fe<sub>2</sub>O<sub>3</sub> partially dissolved and produces Fe<sup>3+</sup> ions. Fe<sup>3+</sup> ions on the surface of Fe<sub>2</sub>O<sub>3</sub>, together with PVP, jointly induce the adsorption of 3,4-ethylenedioxythiophene on the surface of Fe<sub>2</sub>O<sub>3</sub>. PEDOT and Pt nanoparticles are continuously deposited on the core, and finally Fe<sub>2</sub>O<sub>3</sub>@PEDOT/Pt nanocomposites is obtained. Confinement of the Pt nanoparticles in the shell of the conductive polymer PEDOT, and the strong coordination of sulfur atoms to Pt atoms efficiently improve the stability of Pt nanoparticles. In addition, the small-size Pt nanoparticles and the ultra-thin shell layer endow the catalysts with high activity. The nanocatalyst reveals outstanding activity and high stability for the reduction of nitroaromatics.

## EXPERIMENTAL

### Materials

Ferric chloride hexahydrate (FeCl<sub>3</sub>·6H<sub>2</sub>O, AR), polyvinylpyrrolidone (PVP, AR, Mw = 58000), potassium dihydrogen phosphate (KH<sub>2</sub>PO<sub>4</sub>, AR), 2-amino-5-

nitrophenol (99%), 4-Nitroaniline (4-NA, 99%), 2-nitroaniline (2-NA, 99%) and 2-nitrophenol (2-NP, 99%) were purchased from Aladdin Reagent (Shanghai) Co., Ltd. Ethanol (>99.7%) was acquired from Tianjin Guangfu Technology Development Co., Ltd. 3,4-ethylenedioxythiophene (99%) and sodium hydroxide (NaOH) were obtained from Shanghai Macklin Biochemical Technology Co., Ltd. Potassium chloride (K<sub>2</sub>PtCl<sub>4</sub>, 99%) was gained from Shanghai Civic Chemical Technology Co., Ltd. Sodium borohydride (NaBH<sub>4</sub>, ≥98%) and 4-nitrophenol (4-NP, 99%) were provided by Alfa Aesar (Tianjin) Chemical Co., Ltd.

### Preparation of Fe<sub>2</sub>O<sub>3</sub> nanoparticles

Fe<sub>2</sub>O<sub>3</sub> nanoparticles were synthesized by the hydrothermal method according to the literature [27]. FeCl<sub>3</sub>·6H<sub>2</sub>O powder (1.8921 g) was firstly dispersed into an aqueous KH<sub>2</sub>PO<sub>4</sub> solution (350 mL, 4.5×10<sup>-4</sup> M). After mechanically stirring for 1 h at 50 °C, the solution was transferred into a 100 mL polytetrafluoroethylene lined steel reactor and react for 48 hours at 105 °C. Subsequently, the cooled product was rinsed three times with distilled water, and dried at 60 °C for 12 h for further use.

### Preparation of Fe<sub>2</sub>O<sub>3</sub>@PEDOT/Pt catalyst

The Fe<sub>2</sub>O<sub>3</sub>@PEDOT/Pt catalyst was fabricated by a one-step simultaneous redox deposition. Fe<sub>2</sub>O<sub>3</sub> (0.1 g) was firstly dissolved into an aqueous PVP solution (20 mL, 25 g/L) with the aid of ultrasonication, then were vigorously shaken for 24 hours at 25°C to adsorb PVP molecules. Afterwards, PVP-modified Fe<sub>2</sub>O<sub>3</sub> nanoparticles were washed with distilled water three times to remove excess PVP molecules. PVP-modified Fe<sub>2</sub>O<sub>3</sub> nanoparticles were re-dispersed into a four-necked flask with 150 mL distilled water via ultrasonication, followed by the adding of 0.08 mL 3,4-ethylenedioxythiophene monomer, the dispersion was mechanically stirred for 12 hours at room temperature to adsorb 3,4-ethylenedioxythiophene monomer. Subsequently, a certain amount of K<sub>2</sub>PtCl<sub>4</sub> aqueous solution (6.9 mL, 9.6 mM) was added to the system to trigger the redox reaction between 3,4-ethylenedioxythiophene monomer and K<sub>2</sub>PtCl<sub>4</sub>. The redox reaction was carried out at 60 °C for 12 hours. The obtained product was rinsed with water and ethanol three times, and dried at 60 °C for 12 hours.

### Catalytic performance

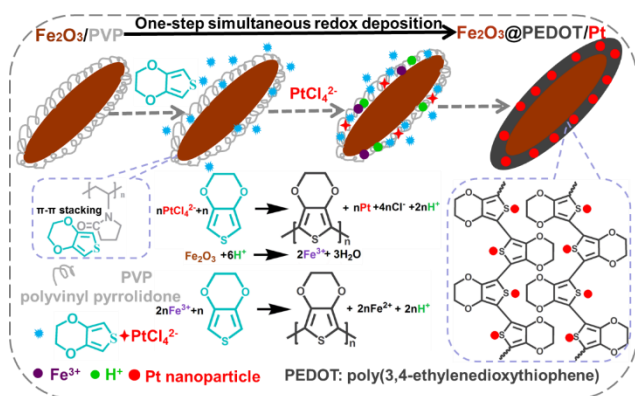
The catalytic performance of Fe<sub>2</sub>O<sub>3</sub>@PEDOT/Pt was assessed through the reduction of nitroaromatic compounds. Taking the reduction reaction of 4-NA as an example, the catalytic activity of the catalyst was examined. Typically, an alcohol solution of 4-NA (2 mL, 5 mM) was mixed with fresh NaBH<sub>4</sub> aqueous solution (20 mL, 200mM), and then the catalyst suspension (0.1 mL, 0.01 wt%, 0.052 mol%) was added. Take 1 mL of this dispersions and 2 mL of distilled water into the cuvette every few minutes, the catalytic activity of the catalyst was evaluated by an

ultraviolet spectrophotometer to monitor the change in the absorbance of 4-NA over time.

The stability was also tested by the reduction of 4-NA. Firstly, an alcohol solution of 4-NA (2 mL, 5 mM) was mixed with fresh  $\text{NaBH}_4$  aqueous solution (20 mL, 200 mM), followed by the addition of catalyst suspensions (1 mL, 0.1wt%). When the reaction was complete, the catalyst was recovered by centrifugation. The next catalysis was carried out under the same conditions, and the cycle was repeated 5 times.

### Characterization

Transmission electron microscopy (TEM) and high-resolution TEM (HRTEM) imaging was carried out using HITACHI HT770 at 100 KV and TECNAI F20 at 200 kV, respectively. Powder X-ray diffraction measurement was performed on a RIGAKU X-ray diffractometer with  $\text{Cu K}\alpha$  radiation ( $\lambda=0.15418$  nm) at 40 kV. FT-IR spectra of the samples were obtained on a Nicolet IS10 infrared spectrometer by the KBr pellet method. An ultraviolet-visible (UV-Vis) spectrophotometer (Shimadzu UV 2550) was utilized to obtain the absorption spectra of different nitroaromatic compounds. X-ray photoelectron spectroscopy (XPS) were performed by an ESCALAB 250 Xi XPS system, where the excitation source is monochromatic  $\text{Al-K}\alpha$  ray ( $h\nu = 1486.6$  eV). The Pt content in the sample was analysed using inductively coupled plasma atomic emission spectroscopy (ICP-AES, AGILENT-725).



**Scheme 1.** Synthetic illustration of  $\text{Fe}_2\text{O}_3$ @PEDOT/Pt nanocomposites

## RESULTS AND DISCUSSION

The preparation procedure of the  $\text{Fe}_2\text{O}_3$ @PEDOT/Pt is schematically illustrated in **Scheme 1**. The spindle-type  $\text{Fe}_2\text{O}_3$  was firstly synthesized by a one-step hydrothermal method [27]. PVP molecules are adsorbed to the surface of  $\text{Fe}_2\text{O}_3$  through hydrogen bonds to form  $\text{Fe}_2\text{O}_3$ /PVP. The PVP molecules modified on  $\text{Fe}_2\text{O}_3$  are combined with 3,4-ethylenedioxythiophene monomer by a  $\pi$ - $\pi$  stacking interaction, which is beneficial for the adsorption of 3,4-ethylenedioxythiophene monomer on the surface of  $\text{Fe}_2\text{O}_3$ . The redox reaction between  $\text{K}_2\text{PtCl}_4$  and 3,4-

ethylenedioxythiophene monomers makes PEDOT and Pt nanoparticles simultaneously deposited on the surface of  $\text{Fe}_2\text{O}_3$  core. At the same time, the generated hydrochloric acid during the redox process can partially dissolve  $\text{Fe}_2\text{O}_3$  to produce a small amount of  $\text{Fe}^{3+}$ . The redox reaction among  $\text{K}_2\text{PtCl}_4$ ,  $\text{Fe}^{3+}$ , and 3,4-ethylenedioxythiophene monomers renders PEDOT/Pt to be continuously and simultaneously deposited on the inner  $\text{Fe}_2\text{O}_3$  core, and finally  $\text{Fe}_2\text{O}_3$ @PEDOT/Pt nanocomposites is obtained.

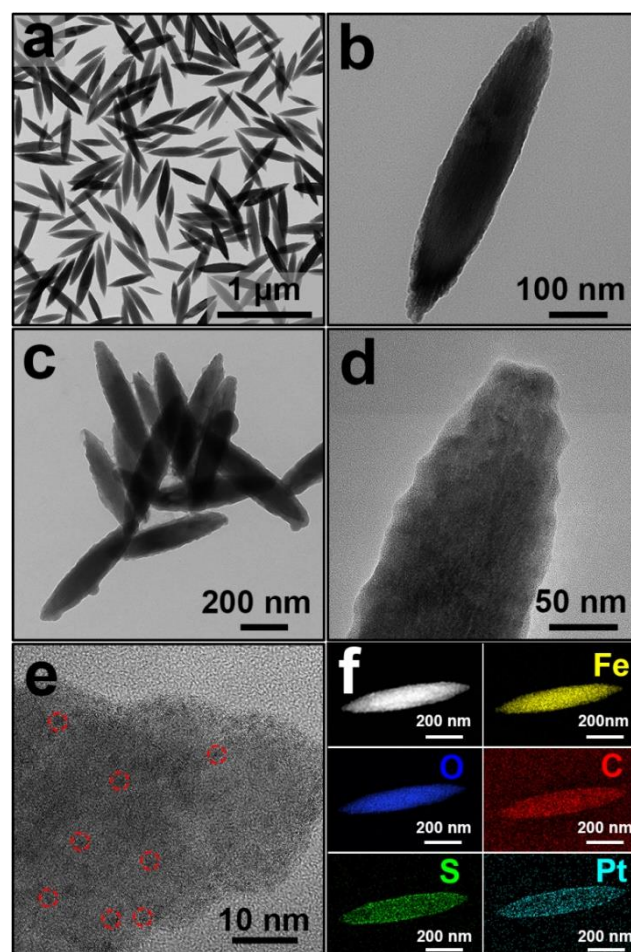


**Fig. 1.** (a, b) TEM images of  $\text{Fe}_2\text{O}_3$ ; (c) TEM image of  $\text{Fe}_2\text{O}_3$ @PEDOT/Pt; (d, e) high resolution transmission electron microscope (HRTEM) image of  $\text{Fe}_2\text{O}_3$ @PEDOT/Pt; (f) HAADF-STEM and EDS elemental mapping images of  $\text{Fe}_2\text{O}_3$ @PEDOT/Pt.

According to the previously reported literature, the spindle-type  $\text{Fe}_2\text{O}_3$  nanoparticles were prepared based on a one-step hydrothermal strategy. Then,  $\text{Fe}_2\text{O}_3$ @PEDOT/Pt was synthesized by a one-step redox deposition strategy. **Fig. 1(a-b)** demonstrates the TEM images of  $\text{Fe}_2\text{O}_3$  nanoparticles. According to a uniform spindle shape of the  $\text{Fe}_2\text{O}_3$  nanoparticles with long axis of about 570 nm and short axis of about 114 nm, the axial ratio was determined to be 5. As shown in **Fig. 1(c-d)**, a layer of polymer shell was successfully coated on the surface of the  $\text{Fe}_2\text{O}_3$  core to construct a spindle-shaped core-shell  $\text{Fe}_2\text{O}_3$ @PEDOT/Pt

catalyst. It should be mentioned that the core-shell interface is not very clear. Moreover, the thickness of PEDOT shell layer is less than 10 nm, which is favorable for the sufficient collision between the substrate and the noble metal nanoparticles and in turn improves the catalytic activity. As displayed in Figure 1e that Pt nanoparticles with small-size less than 2 nm are highly dispersed in the polymer shell structure, which can expose more active sites and endow the catalysts with high activity. EDS mapping images (Fig. 1(f)) show the uniform distribution of Pt species in the spindle-shaped core-shell Fe<sub>2</sub>O<sub>3</sub>@PEDOT/Pt catalyst, which further confirms that the small-size Pt nanoparticles are highly encapsulated into the thin PEDOT shell.

The crystal structures of the samples were characterized by XRD. As presented in Fig. 2(a), the 2θ angles at 24.1°, 33.2°, 35.6°, 40.9°, 49.5°, 54.1°, 57.6°, 62.4°, and 64.0° can be assigned to the (012), (104), (110), (113), (024), (116), (018), (214) and (300) planes of Fe<sub>2</sub>O<sub>3</sub> (JCPDS No. 33-0664) [28-30], suggesting that crystalline Fe<sub>2</sub>O<sub>3</sub> maintains unchanged during the preparation of the catalyst. In addition, no characteristic diffraction peaks of Pt nanocrystals are found in the diffraction pattern of Fe<sub>2</sub>O<sub>3</sub>@PEDOT/Pt, which possibly because the particle size of Pt nanocrystals is too small and Pt nanocrystals are highly dispersed into the polymer shell structure.

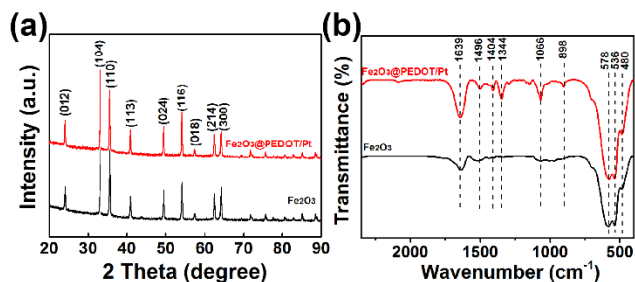


Fig. 2. (a) XRD patterns; (b) FTIR spectra of Fe<sub>2</sub>O<sub>3</sub> and Fe<sub>2</sub>O<sub>3</sub>@PEDOT/Pt

The FTIR measurement was performed to analyse the characteristic functional groups of the samples. Fig. 2(b) shows the FT-IR spectra of the Fe<sub>2</sub>O<sub>3</sub> and Fe<sub>2</sub>O<sub>3</sub>@PEDOT/Pt. The three characteristic peaks of samples at 480, 536, and 578 cm<sup>-1</sup> could be assigned to stretch vibration of the Fe-O in Fe<sub>2</sub>O<sub>3</sub> [31-32]. The peak at 1496 cm<sup>-1</sup> corresponds to C-N stretch vibration of N-C=O moiety [33]. The peak at 1639 cm<sup>-1</sup> can be assigned to the C=O stretching vibration in PVP [34]. When the conductive polymer PEDOT is coated on the surface of Fe<sub>2</sub>O<sub>3</sub>, four new characteristic peaks appear, among which the peak at 898 cm<sup>-1</sup> corresponds to C-S-C stretch vibration, the peak at 1066 cm<sup>-1</sup> is the stretch vibration of C-O-C [35], the peak at 1344 cm<sup>-1</sup> corresponds to C-C stretch vibration of the thiophene ring [36], and the peak at 1404 cm<sup>-1</sup> is the -CH<sub>2</sub>-deformed bending vibration. In addition, after coating the conductive polymer PEDOT, the relative intensity of characteristic peaks at 1496 and 1639 cm<sup>-1</sup> increases, which can be attributed to the common peaks of C-N stretch vibration and C=C stretch vibration in the thiophene ring

[36], combined C=O and C=C stretching vibration in the thiophene ring, respectively. The results mentioned above demonstrate that the conductive polymer PEDOT is effectively coated on the surface of the Fe<sub>2</sub>O<sub>3</sub> core.

In order to further investigate the element composition of the sample and the chemical state of the Pt element, we performed XPS testing on the catalysts Fe<sub>2</sub>O<sub>3</sub>@PEDOT/Pt. As shown in Fig. 3(a), the species of O, C, S, and Pt were observed in the survey spectrum, which is consistent with the EDS elemental mapping image (Fig. 1(f)), suggesting that the conductive polymer PEDOT successfully coated on the Fe<sub>2</sub>O<sub>3</sub> surface to form a core-shell structure and the presence of Pt nanoparticles. There is no Fe peak in the XPS spectrum, which may be due to the limited detection depth of the XPS test. As shown in Fig. 3(c), the O 1s high-resolution spectrum can be deconvoluted into two peaks centred at 532.3 eV and 533.5 eV, which corresponds to C=O in PVP [37] and C-O-C [38], respectively. As displayed in Fig. 3(d), the five peaks in the C 1s high-resolution XPS spectrum centred at 284.6, 285.1, 285.8, 286.6, and 288.9 eV can be ascribed to C-C/C-H, C-S-C, O-C=C, C-O-C, and C=O, respectively. As shown in Fig. 3(e), there are four peaks for S in the catalysts. The peaks at 165.2 eV (S 2p<sub>1/2</sub>) and 164.0 eV (S 2p<sub>3/2</sub>) arise from sulfur atoms in C-S-C [39-40], and the peaks located at 164.4 eV and 163.2 eV correspond to Pt-coordinated S 2p<sub>1/2</sub> and 2p<sub>3/2</sub>, respectively, which further proved the formation of PEDOT on the Fe<sub>2</sub>O<sub>3</sub> surface. The fine XPS spectrum of Pt (Fig. 3(f)) revealed a spin-split doublet, namely, Pt 4f<sub>5/2</sub> (75.7 eV) and 4f<sub>7/2</sub> (72.3 eV), with a 3.4 eV energy split, corresponding to the characteristic peaks of neutral Pt [40]. Compared with the binding energy of traditional Pt nanoparticles, the binding energy of Pt is higher, and the possible reasons for the higher binding energy are as follows: firstly, S is coordinated with Pt, and part of the electrons of Pt is transferred to S; secondly, the smaller size of Pt nanoparticles leads to a higher binding energy of Pt [41].

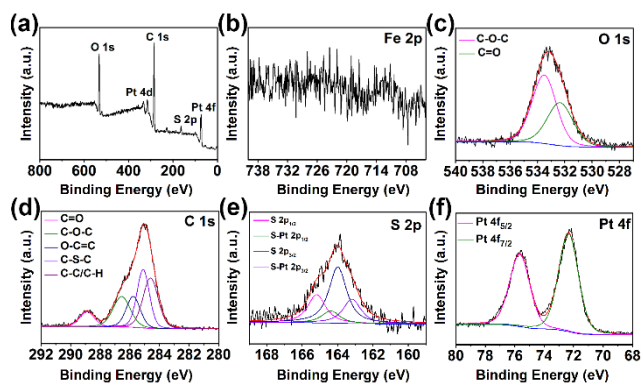


Fig. 3. (a) full survey XPS spectrum of the Fe<sub>2</sub>O<sub>3</sub>@PEDOT/Pt and fine XPS spectra of (b) Fe 2p, (c) O 1s, (d) C 1s, (e) S 2p, (f) Pt 4f

The catalytic properties of Fe<sub>2</sub>O<sub>3</sub>@PEDOT/Pt catalyst were investigated by a common model reduction reaction from 4-nitroaniline (4-NA) to 4-phenylenediamine using an

aqueous  $\text{NaBH}_4$  solution as the reductant at room temperature. There is no any obvious color evolution for the mixture of 4-NA and  $\text{NaBH}_4$  for several days without the catalyst, suggesting that the reaction was difficult to occur without the catalyst. After addition of the dispersion of  $\text{Fe}_2\text{O}_3@$ PEDOT/Pt (0.1 mL, 0.052 mol%) into the above solution, the characteristic absorption intensity of 4-NA at 380 nm in the UV-vis spectra quickly decrease with the prolonged reaction time (Fig. 4(a)), accompanying the color change of yellow to colorless gradually, which manifests the complete reduction of 4-NA. Besides, the occurrence of isosbestic points in the time-dependent UV-vis spectra demonstrate exclusive reduction of 4-NA to 4-phenylenediamine almost without any by product [42]. Although the conversion of 4-NA to 4-phenylenediamine is thermodynamically favoured when  $\text{NaBH}_4$  is used as the reductant, the potential difference between the electron donor and the acceptor is relatively large, so the reaction is relatively slow in terms of kinetics [43].

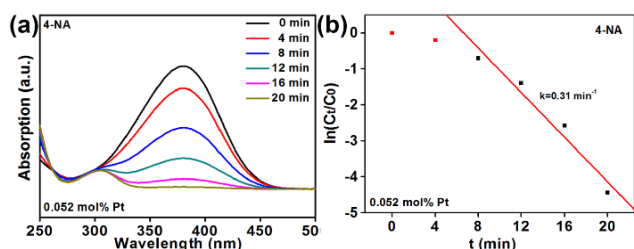


Fig. 4. (a) Time-dependent UV-vis spectrum of 4-NA catalysed by  $\text{Fe}_2\text{O}_3@$ PEDOT/Pt; (b) the plot of  $\ln(C_t/C_0)$  against the reaction time ( $t$ ) for the reduction of 4-NA.

In this study, the concentration of sodium borohydride (200 mM) is much higher than that of the 4-NA (5 mM), so the reduction reaction can be regarded as a pseudo-first-order reaction [44-46]. Fig. 4(b) shows the corresponding first-order kinetic curve. The reaction has a certain induction period, which may be attributed to the time needed for diffusion of 4-NA through the polymer shell to interact with the catalyst surface before the initiation of the reaction [47]. Moreover, first-order kinetic curve excludes the point of the induction period when fitting. The linear relationship between  $\ln(C_t/C_0)$  and the reaction time  $t$  is displayed in Fig. 4(b), where  $C_0$  and  $C_t$  correspond to the absorbance of 4-NA at 0 and  $t$  min, respectively. According to the first order kinetic equation  $\ln(C_t/C_0) = -kt + b$ , the kinetic reaction rate constant  $k$  was determined to be  $0.31 \text{ min}^{-1}$ . Turnover frequency (TOF) measures the rate at which a catalyst catalyzes a reaction, indicating the intrinsic activity of the catalyst, and it could be calculated from the equation S1. According to the equation, the TOF of the  $\text{Fe}_2\text{O}_3@$ PEDOT/Pt catalyst for the reduction of 4-NA is up to  $7331 \text{ h}^{-1}$ , indicating that  $\text{Fe}_2\text{O}_3@$ PEDOT/Pt nanocomposite is effective for the reduction of 4-NA. Furthermore, other nitroaromatic compounds, such as 2-Amino-5-nitrophenol, 2-NA, 2-NP and 4-NP have also been tested for evaluating the catalytic activity of

$\text{Fe}_2\text{O}_3@$ PEDOT/Pt based on the time-dependent UV-vis spectra in Fig. S1-S4, and the TOF is  $3408 \text{ h}^{-1}$ ,  $6003 \text{ h}^{-1}$ ,  $5154 \text{ h}^{-1}$ ,  $2147 \text{ h}^{-1}$ , respectively, as shown in Table 1. In addition, the TOF of some reported heterogeneous catalysts for catalytic reduction of 4-NP and 4-NA are listed in Table. S1 to highlight the excellent activity of the  $\text{Fe}_2\text{O}_3@$ PEDOT/Pt. The excellent catalytic activity of our catalyst in this work might be attributed to the following reasons [48-49]. Firstly, the polymer shell is beneficial for the adsorption of 4-NA because of  $\pi$ - $\pi$  electron interactions between 4-NA and EDOT units, thus enriching 4-NA around the catalyst. Secondly, the highly dispersed and tiny Pt NPs provide more active sites for the catalysis. Finally, the synergetic effect caused by electron transfer between Pt and S improves the catalytic activity.

Table 1. Catalytic performance of  $\text{Fe}_2\text{O}_3@$ PEDOT/Pt for the reduction of different nitromatics.

Entry	Substrate	Time (min)	Conversion (%)	Selectivity (%)	TOF ( $\text{h}^{-1}$ )
1	4-NA	20	98.8	>99	7331
2	2-Amino-5-nitrophenol	36	93.3	>99	3137
3	2-NA	20	95.6	>99	6003
4	2-NP	25	96.0	>99	5154
5	4-NP	48	93.4	>99	2147

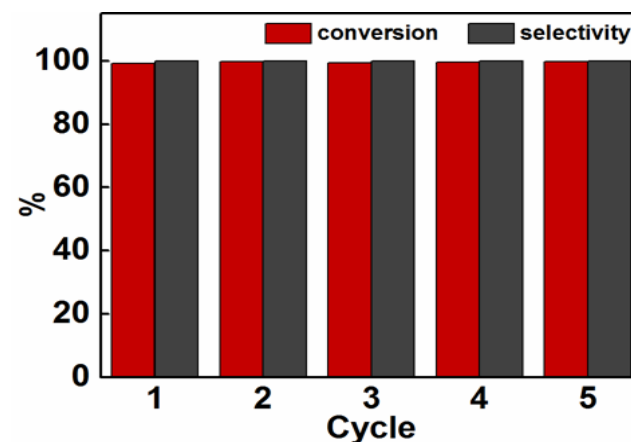


Fig. 5. Conversion and selectivity of 4-NA catalysed by  $\text{Fe}_2\text{O}_3@$ PEDOT/Pt.

The stability of the catalyst is a vital issue in practical applications. Therefore, the reduction of 4-NA by  $\text{NaBH}_4$  was also used to investigate the stability of the  $\text{Fe}_2\text{O}_3@$ PEDOT/Pt catalyst. After the first catalytic reaction, the catalyst was recovered, and the catalytic reaction was performed 5 times under the same conditions. As revealed in Fig. 5, the recovered nanocatalyst after five cycles still shows a stable conversion above 99% and selectivity above 99%, indicating relatively good stability of the  $\text{Fe}_2\text{O}_3@$ PEDOT/Pt. As a result, the  $\text{Fe}_2\text{O}_3@$ PEDOT/Pt nanocatalyst can be used as an efficient

heterogeneous catalyst with good stability, owing to the confinement effect of the protective polymer shell.

## CONCLUSION

In conclusion, we have proposed a simple one-step simultaneous redox deposition strategy to synthesize  $\text{Fe}_2\text{O}_3@\text{PEDOT}/\text{Pt}$  nanocatalyst with tiny Pt nanoparticles highly dispersed in the polymer shell structure. The confinement effect of the polymer shell prevents the migration and agglomeration of Pt nanoparticles during the catalysis process and improves the stability of the catalyst. Tiny Pt nanoparticles confined with thin polymer shell endow the catalysts with high activity. When the catalyst is used to the reduction reaction of nitroaromatic compounds, it shows outstanding catalytic activity with TOF for the reduction of 4-NA up to  $7331\text{ h}^{-1}$  and relatively good stability with any obvious activity loss after five catalytic cycles. The synthesis method of the core-shell nanocatalyst with spatially confined noble metal nanoparticles is simple, and it solves the problem of poor compatibility between the inorganic core, the polymer shell, and the noble metal nanoparticles confined in the shell material to some extent. Furthermore, our strategy could also be extended to one-step preparation of  $\text{Fe}_2\text{O}_3@\text{Polymer}/\text{Pt}$  hybrid materials with core-shell structure.

## ACKNOWLEDGEMENTS

This study was granted by Natural Science Foundation of Hebei Province (No. E2022203082).

## CONFLICTS OF INTEREST

The authors declare no competing interests.

## SUPPORTING INFORMATION

Supporting informations are available online at journal website.

## REFERENCES

- Zhang, L.; Zhou, M.; Wang, A.; Zhang, T.; *Chem. Rev.*, **2020**, 120, 683.
- Dimitratos, N.; Lopez-Sanchez, J. A.; Hutchings, G. J.; *Chem. Sci.*, **2012**, 3, 20.
- Bai, L.; Zhang, S.; Chen, Q.; Gao, C.; *ACS Appl. Mater. Interfaces*, **2017**, 9, 9710.
- Costa, N. J.; Kiyohara, P. K.; Monteiro, A. L.; Coppel, Y.; Philippot, K.; Rossi, L. M.; *J. Catal.*, **2010**, 276, 382.
- Luo, S.; Zeng, Z.; Zeng, G.; Liu, Z.; Xiao, R.; Chen, M.; Tang L.; Tang W.; Lai C.; Cheng M.; Shao B.; Liang Q.; Wang H.; Jiang, D.; *ACS Appl. Mater. Interfaces*, **2019**, 11, 32579.
- Chen, C.; Nan, C.; Wang, D.; Su, Q.; Duan, H.; Liu, X.; Zhang L.; Chu D.; Song W.; Peng Q.; Li, Y.; *Angew. Chem. Int. Ed.*, **2011**, 50, 3725.
- Chen, J.; Wang, D.; Qi, J.; Li, G.; Zheng, F.; Li, S.; Zhao H.; Tang, Z.; *Small*, **2015**, 11, 420.
- Li, G.; Tang, Z.; *Nanoscale*, **2014**, 6, 3995.
- Wang, S.; Zhang, M.; Zhang, W.; *ACS Catal.*, **2011**, 1, 207.
- Luo, Y.; Yang, Q.; Nie, W.; Yao, Q.; Zhang, Z.; Lu, Z. H.; *ACS Appl. Mater. Interfaces*, **2020**, 12, 8082.
- Wang, S.; Zhao, Q.; Wei, H.; Wang, J. Q.; Cho, M.; Cho, H. S.; Terasaki O.; Wan, Y.; *J. Am. Chem. Soc.*, **2013**, 135, 11849.
- Zhu, Y.; Wang, W. D.; Sun, X.; Fan, M.; Hu, X.; Dong, Z.; *ACS Appl. Mater. Interfaces*, **2020**, 12, 7285.
- Joo, S. H.; Park, J. Y.; Tsung, C. K.; Yamada, Y.; Yang, P.; Somorjai, G. A.; *Nat. Mater.*, **2009**, 8, 126.
- Qi, J.; Chen, J.; Li, G.; Li, S.; Gao, Y.; Tang, Z.; *Energy Environ. Sci.*, **2012**, 5, 8937.
- Sun, Z.; Yang, J.; Wang, J.; Li, W.; Kaliaguine, S.; Hou, X.; Deng Y.; Zhao, D.; *J. Mater. Chem. A*, **2014**, 2, 6071.
- Han, J.; Lu, S.; Jin, C.; Wang, M.; Guo, R.; *J. Mater. Chem. A*, **2014**, 2, 13016.
- Zhao, M.; Yuan, K.; Wang, Y.; Li, G.; Guo, J.; Gu, L.; Hu W.; Zhao H.; Tang, Z.; *Nature*, **2016**, 539, 76.
- Chen, X.; Zhang, Y.; Zhao, Y.; Wang, S.; Liu, L.; Xu, W.; Guo Z.; Wang S.; Liu Y.; Zhang, J; *Inorg. Chem.*, **2019**, 58, 12433.
- Long, Y.; Song, S.; Li, J.; Wu, L.; Wang, Q.; Liu, Y.; Jin R.; Zhang, H.; *ACS Catal.*, **2018**, 8, 8506.
- Lin, L.; Zhang, T.; Zhang, X.; Liu, H.; Yeung, K. L.; Qiu, J.; *Ind. Eng. Chem. Res.*, **2014**, 53, 10906.
- Wang, Y.; Biradar, A. V.; Duncan, C. T.; Asefa, T.; *J. Mater. Chem.*, **2010**, 20, 7834.
- Guo, C.; Liang, C.; Qin, X.; Gu, Y.; Gao, P.; Shao, M.; Wong, W. T.; *ACS Appl. Nano Mater.*, **2020**, 3, 7242.
- Wen, F.; Zhang, W.; Wei, G.; Wang, Y.; Zhang, J.; Zhang, M.; Shi, L.; *Chem. Mater.*, **2008**, 20, 2144.
- Han, J.; Wang, M.; Hu, Y.; Zhou, C.; Guo, R.; *Prog. Polym. Sci.*, **2017**, 70, 52.
- Xu, P.; Han, X.; Zhang, B.; Du, Y.; Wang, H. L.; *Chem. Soc. Rev.*, **2014**, 43, 1349.
- Yang, L.; Zhang, Z.; Nie, G.; Wang, C.; Lu, X.; *J. Mater. Chem. A*, **2015**, 3, 83.
- Ozaki, M.; Kratochvil, S.; Matijević, E.; *J. Colloid Interface Sci.*, **1984**, 102, 146.
- Cao, K.; Jiao, L.; Liu, H.; Liu, Y.; Wang, Y.; Guo, Z.; Yuan, H.; *Adv. Energy Mater.*, **2015**, 5, 1401421.
- Kong, D.; Cheng, C.; Wang, Y.; Liu, B.; Huang, Z.; Yang, H. Y.; *J. Mater. Chem. A*, **2016**, 4, 11800.
- Zhou, N.; An, Q.; Xiao, Z.; Zhai, S.; Shi, Z.; *RSC Adv.*, **2017**, 7, 45156.
- Xia, L.; Ju, J. G.; Xu, W.; Ding, C. K.; Cheng, B. W.; *Mater. Des.*, **2016**, 96, 439.
- Yang, Q.; Wu, X.; Huang, X.; Liao, S.; Liang, K.; Yu, X.; Li K.; Zhi C.; Zhang H.; Li, N. *ACS Appl. Mater. Interfaces*, **2019**, 11, 30801.
- Su, N.; Gao, X.; Chen, X.; Yue, B.; He, H.; *J. Catal.*, **2019**, 367, 244.
- He, J.; Su, J.; Wang, J.; Zhang, L.; *Org. Electronics*, **2018**, 53, 117.
- Mitraka, E.; Jafari, M. J.; Vagin, M.; Liu, X.; Fahlman, M.; Ederth, T.; Berggren M.; Jonsson M. P.; Crispin, X.; *J. Mater. Chem. A*, **2017**, 5, 4404.
- Srinivasan, N.; Shiga, Y.; Atarashi, D.; Sakai, E.; Miyauchi, M.; *Appl. Catal., B*, **2015**, 179, 113.
- Zhang, A.; Liu, B.; Liu, S.; Li, M.; Zheng, W.; Deng, L.; Liu, J.; *Chem. Eng. J.*, **2019**, 371, 876.
- D'Arcy, J. M.; El-Kady, M. F.; Khine, P. P.; Zhang, L.; Lee, S. H.; Davis, N. R.; Liu D. S.; Yeung M. T.; Kim S. Y.; Turner C. L.; Lech A. T.; Hammond P. T.; Kaner, R. B.; *ACS Nano*, **2014**, 8, 1500.
- Hu, X.; Xiong, W.; Wang, W.; Qin, S.; Cheng, H.; Zeng, Y.; Wang B.; Zhu, Z.; *ACS Sustainable Chem. Eng.*, **2016**, 4, 1201.
- Fan, J. J.; Fan, Y. J.; Wang, R. X.; Xiang, S.; Tang, H. G.; Sun, S. G.; *J. Mater. Chem. A*, **2017**, 5, 19467.
- Kim, Y. T.; Ohshima, K.; Higashimine, K.; Uruga, T.; Takata, M.; Suematsu, H.; Mitani, T.; *Angew. Chem. Int. Ed.*, **2006**, 45, 407.
- Ramezanpour, A.; Karami, K.; Kharaziha, M.; Silvestru, C.; Bayat, P.; *Appl. Organomet. Chem.*, **2021**, 35, e6329.
- Li, B.; Hao, Y.; Shao, X.; Tang, H.; Wang, T.; Zhu, J.; Yan, S.; *J. Catal.*, **2015**, 329, 368-378.
- Narayanan, K. B.; Sakthivel, N. *J. Hazard. Mater.*, **2011**, 189, 519.
- Jiao, J.; Wang, H.; Guo, W.; Li, R.; Tian, K.; Xu, Z.; Jia Y.; Wu Y.; Cao, L.; *Chem. Asian J.*, **2016**, 11, 3534.
- Zhang, S.; Gai, S.; He, F.; Dai, Y.; Gao, P.; Li, L.; Chen Y.; Yang, P.; *Nanoscale*, **2014**, 6, 7025.
- Das, S. K.; Dickinson, C.; Lafir, F.; Brougham, D. F.; Marsili, E. *Green Chem.*, **2012**, 14, 1322.
- Han, J.; Li, L.; Guo, R; *Macromolecules*, **2010**, 43, 10636.
- Zhao, Y.; Li, Y.; Pang, H.; Yang, C.; Ngai, T.; *J. Colloid Interface Sci.*, **2019**, 537, 262.

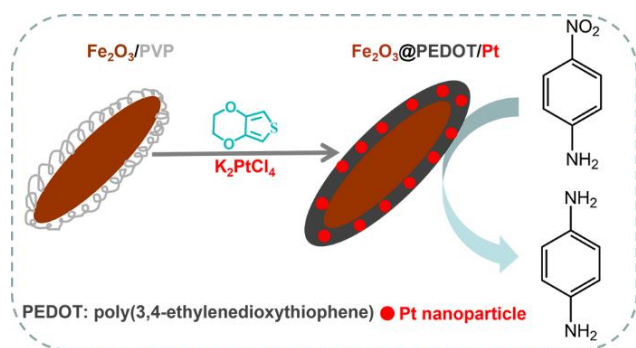
## AUTHORS BIOGRAPHY



**Dr. Wanchun Guo** serves as the Associate Professor of the Department of Applied Chemistry at Yanshan University and Fellow of International Association of Advanced Materials. He received his BS in Materials Chemistry from Tianjin University in 2005, and Ph.D. in Materials Science and Engineering from University of Science and Technology Beijing in 2013. He focused on surfacial and interfacial design of heterogenous atom-doping carbon materials to address crucial challenges in energy and environmental issues.

## Graphical Abstract

We propose a facile one-step simultaneous redox deposition strategy to fabricate core-shell  $\text{Fe}_2\text{O}_3$ @poly(3,4-ethylenedioxythiophene)/Pt ( $\text{Fe}_2\text{O}_3$ @PEDOT/Pt) nanocatalyst with spatially confined Pt nanoparticles. The confinement effect and strong coordination ability of the thin sulfur-enriched polymer shell could prevent the migration and agglomeration of active small-size Pt nanoparticles during the catalytic process and improve the catalyst stability.



This article is licensed under a Creative Commons Attribution 4.0 International License, which allows for use, sharing, adaptation, distribution, and reproduction in any medium or format, as long as appropriate credit is given to the original author(s) and the source, a link to the Creative Commons license is provided, and changes are indicated. Unless otherwise indicated in a credit line to the materials, the images or other third-party materials in this article are included in the article's Creative Commons license. If the materials are not covered by the Creative Commons license and your intended use is not permitted by statutory regulation or exceeds the permitted use, you must seek permission from the copyright holder directly.

Visit <http://creativecommons.org/licenses/by/4.0/> to view a copy of this license.